CHAPTER 8
GEOCHRONOLOGY

Rocks of the Liquiñe area (40°S, Ch. 4.4) were subject of an isotopic study in order to (1) constrain the age of high temperature metamorphism and deformation observed in the country rock of the North Patagonian Batholith (NPB) and (2) to constrain the age of magmatism and low-grade metamorphism manifested in rocks of the Southern Andean back-arc.

8.1 The Rb-Sr system

Rb and Sr are trace elements in the earth. Rb is an alkali element occurring as Rb^+ in nature. Its ionic radius (Rb^+: 1.48 Å) is similar to that of K (K^+: 1.33 Å) which makes it suitable for substituting for K in all K-bearing minerals (e.g. micas, orthoclase, microcline). Rb has two naturally occurring isotopes: ^{85}Rb and ^{87}Rb with natural abundances of ca. 72.2 % and 27.8 %, respectively. ^{87}Rb is radioactive and decays to stable radiogenic ^{87}Sr by emission of a negative beta particle (electron):

$$^{87}Rb \rightarrow {}^{87}Sr + \beta^- + \tilde{n} + Q \qquad \text{(E 8.1)}$$

where β^- is the beta particle, ñ is an antineutrino, and Q is the released decay energy.

Sr is an alkaline earth element generally occurring as Sr^{2+}. Its ionic radius (Sr^{2+} 1.13 Å) is similar to that of Ca (Ca^{2+} 0.99 Å) which it replaces in many minerals (e.g. plagioclase, calcite, epidote, apatite). Sr has four naturally occurring isotopes: ^{88}Sr, ^{87}Sr, ^{86}Sr, and ^{84}Sr with natural abundance of ca. 82.5 %, 7.04 %, 9.87 %, and 0.56 %, respectively.

Rb-Sr isotope geochronology makes use of the radioactive decay of ^{87}Rb to ^{87}Sr following the age equation (e.g. Faure, 1986):

$$^{87}Sr/^{86}Sr = (^{87}Sr/^{86}Sr)_0 + {}^{87}Rb/^{86}Sr\,(e^{\lambda t}-1) \qquad \text{(E 8.2)}$$

where $^{87}Sr/^{86}Sr$ and $^{87}Rb/^{86}Sr$ are respective isotopic ratios observed today, $(^{87}Sr/^{86}Sr)_0$ is the initial Sr ratio at time t = 0, and λ is the decay constant.

8.2 Dating migmatization and deformation in the intra-arc

In the Liquiñe area (40°S) migmatites occur in the roof of a NPB-related Cretaceous batholith in the Pirihueico block (see Ch. 4.4.3). The migmatites form a domal structure with most prominent deformation localized in the flanks of the dome. The migmatitic layering is folded in the central part and shows a mylonitic overprint in the flanks. It was the aim of this study to reveal the temporal relationship between migmatization, pluton emplacement, and wall rock deformation to decide whether these processes are genetically linked (i.e., took place coevally) or are the manifests of significantly distinct events (i.e., separated by time gaps). For this purpose we sampled migmatites and mylonites recording different amounts of strain.

8.2.1 Petrography

The migmatites are medium to coarse grained rocks with a compositional layering (migmatitic layering) defined by several mm-thick quartz-feldspar-muscovite rich and biotite rich layers (Fig. 8.1a). In places, felsic layers are several cm thick suggesting that they represent partial melt segregated from the metamorphic country rock by partial melting. Rotated feldspar clasts up to 3 cm and quartz-feldspar-muscovite boudins up to 30 cm are abundant. In thin section, zircon and apatite are recognized as accessory mineral phases. Quartz generally shows indications for static crystallization like straight grain boundaries and only minor undulose extinction.

The mylonites which developed from this protolith are medium to fine grained, show a penetrative foliation defined by oriented micas, and a weakly developed lineation defined by elongated grains or elongate grain aggregates (Fig.8.1b). Quartz occurs as mm-thick elongate lenses. In thin section, quartz shows indications of crystal plasticity like undulose extinction, deformation bands, and subgrain formation indicating dynamic recrystallization. Big feldspar generally occurs as brittle fractured, passively rotated clasts with kinked or bend twin lamellae. Occasionally, fine grained feldspar occurs around those relic porphyroclasts (core-and-mantle structure) or in pressure shadows indicating at least locally synkinematic feldspar growth. Kinematic indicators like SC and CC´- fabrics, mica fishes, and rotated clasts show dominantly east-up on the western flank and west-up on the eastern flank of the dome.

No clear cross cutting relationship between the migmatitic layering and the mylonitic foliation has been observed in the field. In thin section however, the occurrence of high-T (“magmatic”) relicts like zoned (“patchy”) plagioclase within greenschist facies mylonitic samples indicate that migmatization preceded mylonitization at least locally, i.e. that the rocks experienced a retrograde metamorphic overprint.

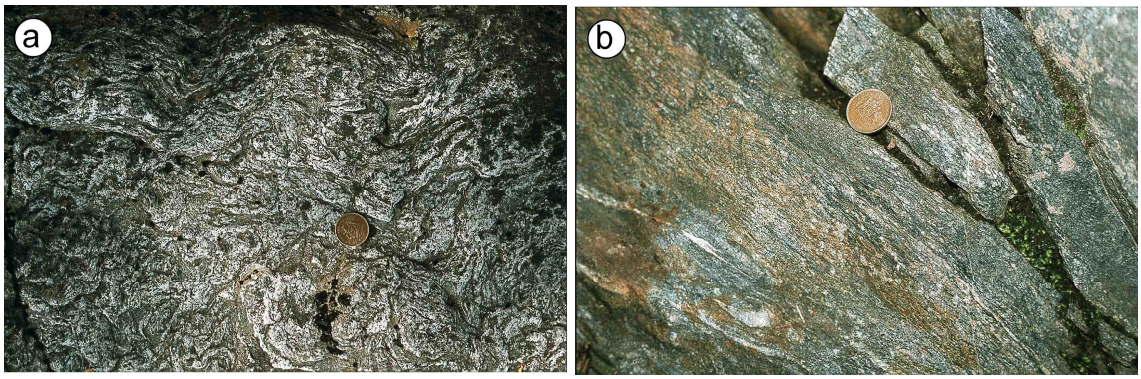

***Fig. 8.1**: (a) Migmatite versus (b) mylonite of the Liquiñe area. Coin for scale.*

8.2.2 Approach

The rocks studied here are migmatites and mylonitized migmatites, i.e. they were formed under retrograde amphibolite to greenschist facies metamorphic conditions. A variety of geochronological tools are available for the direct dating of deformation within ductily deformed rocks. However, the most promising isotopic system for greenschist facies mylonites is the Rb-Sr system applied to white mica-bearing mineral assemblages (e.g. Freemann et al., 1997, 1998, George and Bartlett, 1996, Hetzel and Glodny, 2002). This is mainly because

- White mica is widespread and stable in greenschist facies mylonites
- White mica is fabric forming and can thus easily be linked to deformation
- White mica is relatively stable with respect to sub-greenschist facies alteration and weathering processes (Clauer et al., 1982)
- The Rb-Sr closure temperature (sensu Dodson, 1973) of white mica is ca. 550°C (e.g. Cliff, 1985) and therefore ca. 200°C above the brittle-ductile transition within quartzo-feldspatic rocks at usual strain rates. This is essential because in order to date synkinematically crystallized or recrystallized minerals, the closure temperature must be significantly higher than the synkinematic temperature (Getty and Gromet, 1992).
- White mica equilibrium composition is dependent on the P and T conditions during crystallization thus possibly offering petrological constraints on the timing of formation of chemically different mica generations.

- Several mineral phases are paragenetic with white mica and may serve as contemporary Sr-isotopic reservoirs. Plagioclase generally deforms ductile by dynamic recrystallization at high temperatures (> 500°C, Tullis et al., 2000) and brittle by fracturing at lower temperatures. However, under favorable conditions (e.g. compositional disequilibrium), plagioclase may also recrystallize ("neo-mineralize") during greenschistfacies deformation (Tullis et al., 2000). Relic porphyroclasts in greenschist facies mylonites thus generally constrain the initial Sr isotopic composition of the primary, pre-deformative assemblage. Apatite has been shown to readily recrystallize during greenschist facies mylonitization (Hetzel and Glodny, 2002). In cases where synkinematic recrystallization of plagioclase is incomplete, e.g. during greenschist facies, low-temperature deformation, apatite can thus be used as a proxy for the equilibrium Sr isotopic composition for all synkinematically recrystallizing material.

In order to date migmatization and subsequent greenschist facies deformation, two migmatite samples (LOF84 and LOF41) and five mylonite samples (LOF52, LOF53, LOF54, LOF56, LOF112) were selected for Rb-Sr analysis. The main phases in the samples are quartz, feldspar, white mica, biotite/chlorite, apatite and zircon. All samples show a slight diaphtoritic overprint as indicated by the chloritization of biotite and the sericitization of feldspar.

8.2.3 White mica chemistry

Two different types of white mica grains can be distinguished and related to different fabrics in mylonitic samples: (1) Type 3 grains are small (< 200 µm) and occur along shearplanes (C´ planes) and in pressure shadows of clasts and (2) type 2 grains which are up to 1 mm and occur as elongate in (001) clasts within the quartz-dominated recrystallized matrix and along the mylonitic foliation (C plane). Type 3 grains are thought to be crystallized during deformation whereas type 2 grains are rotated passively and only locally recrystallized. From this relationship, type 2 grains should be at least slightly older than type 3 grains. White mica grains in migmatite samples vary in size from less than 200 µm to more than 1 mm and define the migmatitic layering together with biotite. These high-grade metamorphic white mica grains are referred to as type 1 grains in this study.
After petrographic assessment of textural relationships, the white micas were analyzed for major element composition in order to recognize chemical differences between the different grain types. Chemical differences may indicate the existence of mica

populations which crystallized during different events at significantly different P/T conditions if the mineralogy is favorable (Massonne and Schreyer, 1987).

Analyses were realized at the GeoForschungsZentrum Potsdam (GFZ) on a CAMECA SX100 electron microprobe operating in the wavelength-dispersive mode. A set of natural and synthetic standard minerals was used for calibration, and the PAP program (Pouchou and Pichoir, 1984) for matrix correction. Major and minor elements were analyzed at 15 kV acceleration voltage, 20 nA beam current and 20 to 30 s counting time for major and minor elements, respectively. The beam diameter used for the analyses was 5 µm. Table 8.1 shows microprobe analysis of five mylonite samples (LOF52, LOF53, LOF54, LOF56, LOF112, type 3 and 2 grains not differentiated) and two migmatite samples (LOF41, LOF84, type 1 grains) which were subsequently dated.

	LOF41	**LOF84**	**LOF52**	**LOF53**	**LOF54**	**LOF56**	**LOF112**
Rock type	Migmatite	Migmatite	Mylonite	Mylonite	Mylonite	Mylonite	Mylonite
Mica type	1	1	2/3	2/3	2/3	2/3	2/3
n	9	18	17	17	14	29	28
SiO_2 (wt%)	46.8	46.7	46.3	47.5	48.2	47.4	46.4
TiO_2 (wt%)	0.33	1.24	0.24	0.31	0.80	0.33	0.54
Al_2O_3 (wt%)	34.5	34.2	35.5	36.1	36.5	36.8	35.6
FeO (wt%)	1.33	1.12	0.92	0.99	1.11	0.88	1.22
MnO (wt%)	0.02	0.01	0.01	0.01	0.01	0.01	0.01
MgO (wt%)	0.76	0.70	0.49	0.48	0.52	0.41	0.49
CaO (wt%)	0.01	0.01	0.08	0.02	0.00	0.02	0.07
Na_20 (wt%)	0.38	0.42	0.97	0.71	0.88	0.99	0.72
K_2O (wt%)	10.9	10.6	9.83	10.1	10.1	9.94	10.2
Total	95.0	95.0	94.4	96.2	98.1	96.8	95.3
Si (pfu)	3.124	3.115	3.094	3.112	3.100	3.087	3.082
Ti (pfu)	0.017	0.062	0.012	0.015	0.039	0.016	0.026
Al (pfu)	2.719	2.690	2.798	2.783	2.763	2.821	2.786
Fe (pfu)	0.000	0.000	0.000	0.054	0.060	0.048	0.000
Mn (pfu)	0.000	0.000	0.000	0.000	0.000	0.000	0.000
Mg (pfu)	0.075	0.069	0.049	0.047	0.050	0.040	0.049
Ca (pfu)	0.001	0.000	0.005	0.001	0.000	0.001	0.005
Na (pfu)	0.049	0.054	0.126	0.091	0.109	0.125	0.092
K (pfu)	0.927	0.901	0.838	0.846	0.828	0.826	0.868
Total	6.912	6.891	6.923	6.963	6.948	6.962	6.909

***Tab. 8.1**: Microprobe analyses of white mica from the Liquiñe migmatite dome. Abbreviations: n = number of determinations, wt% = weight percent (water has not been fitted to the totals), pfu = per formula unit (based on 11 O).*

All analyzed white micas are muscovites, i.e. have stoichiometric Si lower than 3.15 per formula unit. The data show that the muscovite chemistry is similar both within and between samples of mylonites (type 3 and 2) and migmatites (type 1). A difference

between samples of mylonites and migmatites are the contents of Na. Na shows slightly higher abundances (by a factor of 2) in type 3 and 2 micas with respect to the type 1 micas, however, the difference may not be significant if the variability of Na compositions in the rocks is considered. This Na enrichment is visualized in Fig. 8.2 which presents the Alkali versus Si variation of the samples. The high Na nature of the micas from mylonitic samples with respect to migmatitic samples is apparently controlled by the whole rock chemistry. Whole rock chemical data of Liquiñe samples (see Tab. A5 in Appendix VI) indicate that mylonites are ca. 1.5 times richer in Na with respect to the migmatitic protolith.

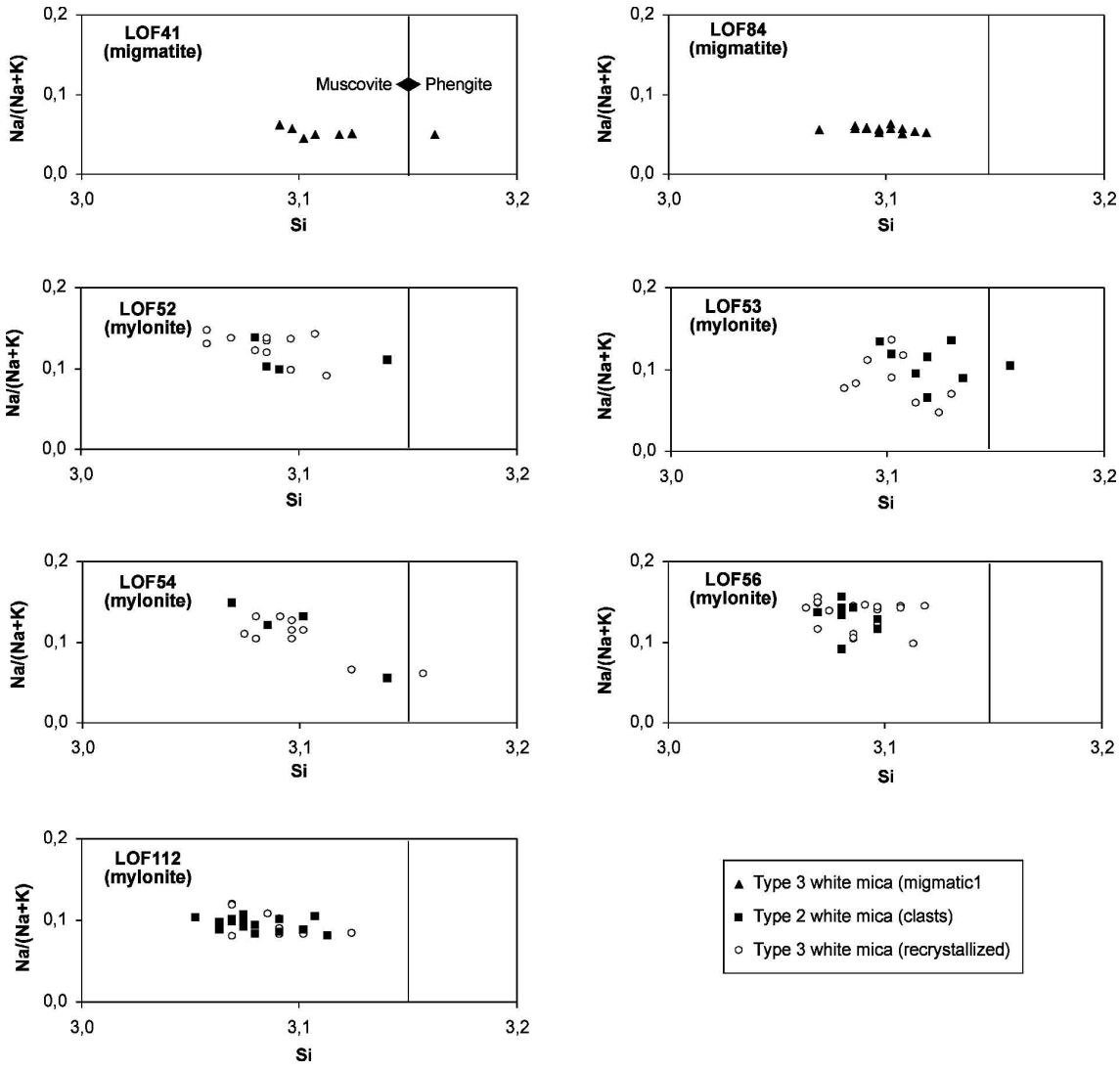

Fig. 8.2: *Alkali versus silica plots for samples of the Liquiñe migmatite dome: LOF41 and LOF84 are migmatites; LOF52, LOF53, LOF54, LOF56, LOF112 are mylonites.*

8.2.4 Analytical technique

Sample preparation and isotope analysis were performed at the GeoForschungsZentrum Potsdam (GFZ).

Sample preparation

For the Rb-Sr isotope analyses, whole rock powder and mineral concentrates of muscovite biotite/chlorite, feldspar, apatite, and quartz were produced. Depending on the rock composition, ca. 400 – 600 g of fresh rock were prepared. After washing in water and acetone, samples were reduced in size by hammering to ca. 1cm^3 sized pieces. Where present, altered pieces were removed. In order to obtain whole rock powder samples, ca. 50 g of rock pieces were powdered in a WIDIA mill for 10 – 15 minutes to less than 100 µm. For mineral concentrates, 200 – 500 g of rock pieces were handcrushed with a steel mortar down to less than 355 µm. The sieve fraction was subsequently washed in water to remove the fine fraction (< ca. 50 µm). Mineral separation was carried out using a Franz isodynamic separator and heavy liquids (bromoform and diiodomethane). Plagioclase concentrates were generally obtained from the Frantz non-magnetic, $\rho \leq 2.84$ g/cm^3 (bromoform) fraction and purified by hand-picking under the binocular microscope. Great care was taken to separate unaltered and inclusion free plagioclase grains. In the case of fine grained samples, plagioclase concentrates were purified by separating it from quartz using a $\rho \approx 2.6$ g/cm^3 bromoform/acetone mixture. Apatite concentrates were obtained from the Frantz non-magnetic, $\rho > 2.84$ g/cm^3 fraction and purified by frictional separation off paper and hand-picking under the binocular microscope. Mica concentrates were obtained from the paramagnetic at 0.25A/13° (biotite) and 0.4-0.9A/13° (muscovite) fractions. Several paramagnetic fractions of muscovite were produced in order to separate eventually existing, chemically different mineral populations. Micas from each paramagnetic fraction were separated further into several sieve fractions (biotite: 100 – 160 µm, muscovite: 100 – 160 µm, 160 – 250 µm, 255 - 355 µm) for the purpose of studying the grain size dependence of isotope systematics. To obtain high purity separates, micas were extracted by frictional separation off paper, which makes use of the adhesive nature of platy minerals. Inclusion-free mica separates were finally obtained by grounding the mica concentrates under pure ethanol in an agate mortar and finally sieving them in ethanol. Where present, Fe/Mn-oxides/hydroxides on muscovites were removed by leaching them for 15-30 minutes in cold 5% aqueous solution of oxalic acid.

Isotope analysis

Samples were analyzed for Rb and Sr isotope contents by isotope dilution methods. They were weighed into Savillex screw-top containers (plagioclase: 10 – 15 mg, apatite: 5 – 8 mg, mica, whole rock: 15 – 20 mg), spiked with a suitable mixed ^{87}Rb-^{84}Sr spike solution, and dissolved in a mixture of 4/5 HF and 1/5 HNO_3 (12 – 24 h at ca. 120°C). Subsequently, the solutions were evaporated and the fluorides converted to chlorides by dissolving them in 6 N HCl (12 – 24 h at ca. 120°C). After subsequent evaporation, the chlorides were taken up in 1 ml 2.5 N HCL. Where present, residual precipitates were separated using a centrifuge.

Solutions were processed by standard cation-exchange techniques using quartz-glass exchange columns filled with DOWEX AG - 50 W*8 cation exchange resin and conditioned with 2.5 N HCL. Rb- and Sr-eluates were obtained with a total of 25 – 30 ml 2.5 N HCL. After evaporation of the Rb- and Sr-eluates, the chlorides (both Sr and Rb: 0.1 – 0.5 µg) were loaded with 0.1 M H_3PO_4 and 1 M H_3PO_4, respectively, onto tantalum filaments.

The determination of Rb and Sr isotopic ratios were performed on a VG Sector 54 multicollector thermal ionization mass spectrometer (TIMS) at the GeoForschungsZentrum Potsdam (GFZ) in static and dynamic mode, respectively. The precision of measurements was controlled by sample duplicates. The accuracy of measurements was monitored on blank solutions and standard reference materials. During the period of laboratory work, 10 measurements of the international standard NBS987 gave an average of $^{87}Sr/^{86}Sr$ ratio of 0.710265 ± 0.000032 (2σ) and 12 measurements on natural Rb gave 2.6068 ± 0.0080 (2σ). To account for mass fractionation, all measured Sr isotopic ratios were normalized to $^{86}Sr/^{88}Sr = 0.1194$ and all measured $^{87}Rb/^{85}Rb$ ratios were multiplicated with a correction factor of 0.995.

Rb-Sr isotope regression lines and ages were calculated using Isoplot/Ex 2.06 (Ludwig, 1999). An analytical uncertainty of 1.5% is assigned to the $^{87}Rb/^{86}Sr$ ratios during the calculations. A standard error of 0.005% is assigned to the $^{87}Sr/^{86}Sr$ ratio during calculation, they are reported, however, with their $2\sigma_m$ internal precision plus uncertainties from spike correction. Calculation was based on a decay constant for ^{87}Rb of $1.42 \cdot 10^{-11}$ a^{-1} (Neumann and Huster, 1974).

8.2.5 Analytical results

Table 8.2 summarizes the Rb-Sr data for the Liquiñe migmatite dome. The majority of mineral isotopic data does not yield isochron ages but show a systematic variation within a given sample:

- The Sr is more radiogenic in coarse grained muscovite than in fine grained muscovite.
- Regarding muscovites of the same grain size, low paramagnetic muscovites are more radiogenic in their Sr than highly paramagnetic muscovites.
- Biotite/chlorite are significantly poorer in radiogenic Sr
- Apatite has mostly a higher amount of radiogenic Sr with respect to plagioclase

Sample LOF41 (UTM 260075E/5595740N) does not yield data fitting on isochrones defined by more than two points (Fig. 8.3a). The oldest apparent mineral age is obtained for coarse grained muscovite (160-250 μm) combined with plagioclase (99.4 ± 1.6 Ma, 2σ), the youngest apparent age is 79.7 ± 1.4 Ma ($2\sigma_m$, $(^{87}Sr/^{86}Sr)_i$ = 0,713400) yielded by fine grained, highly paramagnetic muscovite (100-160 μm, m = 0.5A) and apatite. The whole rock-biotite/chlorite apparent age is 50.1 ± 0.8 Ma (2σ).

Sample LOF84 (UTM 258004E/5595448N) gives isotopic data which suggest the presence of two mica populations which slightly differ in age and chemistry (Fig. 8.3b): Two sieve fractions (100-160 and 160-250μm) of low paramagnetic muscovite (m = 0.8A) together with plagioclase, apatite and the whole rock data yield an regression line corresponding to an age of 107.9 ± 8.1 Ma (2σ, MSWD = 37) whereas two sieve fractions (100-160 and 160-250 μm) of highly paramagnetic muscovite (m = 0.5A) together with plagioclase, apatite and the whole rock data yield an regression line corresponding to an age of 100.2±2.9 Ma (2σ, MSWD = 19, $(^{87}Sr/^{86}Sr)_i$ = 0,713010). Biotite/chlorite plot below these regression lines, the whole rock-biotite/chlorite apparent age is 82.2 ± 1.2 Ma ($2\sigma_m$).

Sample LOF52 (UTM 258387E/5598864N) yield an isochron age of 138.4 ± 1.9 Ma (2σ, MSWD = 1.15) defined by coarse grained muscovite (250-355 μm), plagioclase, and the whole rock data (Fig. 8.3c). Finer grained muscovite fractions plot below this isochron line. The youngest apparent age is 116.4 ± 1.7 Ma (2σ, $(^{87}Sr/^{86}Sr)_i$ = 0,716311) obtained from a combination of fine grained, highly paramagnetic muscovite (100-160

μm, m = 0.6A) and apatite. The whole rock-biotite/chlorite apparent age is 80.3 ± 1.2 Ma (2σ).

Sample LOF53 (UTM 258084E/5595605N) does not yield data defining isochrones with more than two points (Fig. 8.3d). The oldest apparent age is 100 ± 1 Ma (2σ) obtained by coarse grained muscovite (250-355 μm) together with plagioclase, the youngest apparent age is 87.9 ± 1.3 (2σ, $(^{87}Sr/^{86}Sr)_i$ = 0,720332) when using intermediate grained muscovite (160-250μm) and plagioclase which is identical within errors with an apparent age given by plagioclase and fine grained muscovite (100-160μm, 89.6 ± 1.4 Ma, $2\sigma_m$). In contrast to other samples, apatite of sample LOF53 is poorer in ragiogenic Sr than plagioclase suggesting that secondary sub-greenschistfacies alteration processes affected its isotopic composition (see discussion below). For this reason, apatite is not considered during calculations. The whole rock-biotite/chlorite apparent age is 75.9 ± 1.2 Ma (2σ).

Sample LOF54 (UTM 258071E/5595699N) show a systematic variation of isotopic data (Fig. 8.3e, f) where the oldest apparent age defined by coarse grained, low paramagnetic muscovite (250-355 μm, m = 0.8A) is 101.8 ± 1.5 Ma (2σ) and the youngest apparent age is 93.8 ± 1.4 Ma (2σ, $(^{87}Sr/^{86}Sr)_i$ = 0,720251) obtained from a combination of fine grained, highly paramagnetic muscovite (100-160 μm, m = 0.6A) and apatite. The whole rock-biotite/chlorite apparent age is 41.1 ± 0.62 Ma (2σ).

Sample LOF56 (UTM 257555E/5596032N) yields an isochron age of 84 ± 1 Ma (2σ, MSWD = 1.3, $(^{87}Sr/^{86}Sr)_i$ = 0,713398) based on two magnetic fractions of muscovite (m = 0.45 and 0.8A) and apatite (Fig. 8.3g). Plagioclase plots below this isochron suggesting that its Sr isotope composition is inherited. Thus it is not included in the regression calculation which aims to constrain the age of ductile deformation. The whole rock-biotite/chlorite apparent age is 59.1 ± 0.88 Ma (2σ).

Sample LOF112 (UTM258756E/5601717N) gives an regression line, the slope of which correspond to an age of 104.3 ± 4.7 Ma (2σ, MSWD = 13, $(^{87}Sr/^{86}Sr)_i$ = 0.718510) considering four muscovite fractions, plagioclase and the whole rock data (Fig. 8.3h). The fact that plagioclase plots on the isochron indicates that it may have recrystallized during greenschist facies deformation. Like in sample LOF53, apatite of sample LOF112 is poorer in radiogenic Sr, probably due to secondary sub-greenschistfacies alteration processes and thus not included in the calculation. The whole rock-biotite/chlorite apparent age is 76.2 ± 1.2 Ma (2σ).

Deformation		Size (μm)	M (A)	Rb (ppm)	Sr (ppm)	$^{87}Rb/^{86}Sr$	$^{87}Sr/^{86}Sr$	$^{87}Sr/^{86}Sr$ $2\sigma_m$ (%)	Age (Ma, 2σ)
Migmatitic	**LOF84**								
	ms1	160 - 250	0.8	148	118	3.633	0.718669	0.0014	107.9 ± 8.1 Ma (+ms2, plag, ap, wr)
	ms2	100-160	0.8	156	93.4	4.829	0.720333	0.0014	
	ms3	160 - 250	0.5	189	68.1	8.059	0.724550	0.0014	100.2 ± 2.9 Ma (+ms4, plag, ap, wr)
	ms4	100-160	0.5	188	67.0	8.113	0.724499	0.0014	
	bt			462	8.20	167.2	0.908319	0.0012	82.2 ± 1.2 Ma (+wr)
	plag			3.20	177	0.053	0.713034	0.0012	
	ap			1.62	220	0.021	0.713148	0.0020	
	wr			70.6	222	0.922	0.714253	0.0022	
Migmatitic	**LOF41**								
	ms1	160 - 250	0.8	193	54.3	10.32	0.727251	0.0014	99.4 ± 1.6 Ma (+plag)
	ms2	100 - 160	0.8	163	82.2	5.753	0.720397	0.0012	85.9 ± 1.5 Ma (+ap)
	ms3	100 - 160	0.5	170	78.8	6.266	0.720492	0.0016	79.7 ± 1.4 Ma (+ap)
	bt			102	16.3	18.09	0.725846	0.0016	50.88 ± 0.83 Ma (+wr)
	plag			11.8	66.9	0.509	0.713382	0.0012	
	ap			16.9	159	0.307	0.713747	0.0018	
	wr			59.3	139	1.240	0.713668	0.0012	
Low strain	**LOF52**								
	ms1	250-355	0.9	214	60.2	10.30	0.736217	0.0012	137.4 ± 1.9 Ma (+plag, wr)
	ms2	100-160	0.9	218	56.7	11.16	0.735829	0.0012	123.0 ± 1.8 Ma (+ap)
	ms3	100-160	0.6	232	49.4	13.66	0.738910	0.0014	116.4 ± 1.7 Ma (+ap)
	bt			463	6.80	202.8	0.948450	0.0028	80.3 ± 1.2 Ma (+wr)
	plag			10.4	361	0.083	0.716196	0.0014	
	ap			1.58	174	0.026	0.716354	0.0012	
	wr			65.6	161	1.181	0.718310	0.0036	
Low strain	**LOF53**								
	ms1	250-355	0.4	195	52.0	10.87	0.735827	0.0014	100 ± 1 Ma (+plag)
	ms2	160 - 250	0.4	207	61.8	9.695	0.732437	0.0016	87.9 ± 1.3 Ma (+plag)
	ms3	100-160	0.6	201	58.2	10.03	0.733921	0.0018	95.4 ± 1.5 Ma (+plag)
	ms4	100-160	0.4	213	63.8	9.705	0.732682	0.0012	89.6 ± 1.4 Ma (+plag)
	bt			291	43.9	19.24	0.740616	0.0016	75.9 ± 1.2 Ma (+wr)
	plag			6.60	435	0.044	0.720388	0.0014	
	(ap)*			1.10	154	0.077	0.719976	0.0014	
	wr			117	260	1.308	0.721290	0.0020	
Low strain	**LOF54**								
	ms1	250-355	0.8	201	32.9	17.69	0.745887	0.0020	101.8 ± 1.5 Ma (+plag)
	ms2	250-355	0.6	202	34.4	17.08	0.744694	0.0014	100.5 ± 1.5 Ma (+plag)
	ms3	160 - 250	0.8	204	36.1	16.36	0.743440	0.0016	99.7 ± 1.5 Ma (+ap)
	ms4	160 - 250	0.6	206	37.0	16.17	0.742511	0.0016	96.9 ± 1.4 Ma (+ap)
	ms5	100-160	0.8	212	39.4	15.67	0.741707	0.0012	96.4 ± 1.4 Ma (+ap)
	ms6	100-160	0.6	215	40.2	15.50	0.740905	0.0014	93.8 ± 1.4 Ma (+ap)
	bt			310	16.0	56.31	0.753279	0.0014	41.10 ± 0.62 Ma (+wr)
	plag			3.80	58.8	0.185	0.750556	0.0012	
	ap			2.15	173	0.036	0.720299	0.0016	
	wr			85.5	159	1.559	0.721315	0.0018	
High strain	**LOF56**								
	ms1	100-160	0.8	123	75.8	4.718	0.719054	0.0016	84 ± 1 Ma (+ms2, ap)
	ms2	100-160	0.45	141	46.7	8.721	0.723719	0.0020	
	bt			298	10.3	84.64	0.784012	0.0027	59.14 ± 0.88 Ma (+wr)
	(plag)*			6.20	229	0.079	0.713266	0.0012	
	ap			1.14	131	0.025	0.713425	0.0018	
	wr			67.9	235	0.836	0.713598	0.0012	
High strain	**LOF112**								
	ms1	250-355	0.75	173	147	3.426	0.723557	0.0012	104.3 ± 4.7 Ma (+ms2-4, wr, plag)
	ms2	250-355	0.6	173	128	3.904	0.724160	0.0018	
	ms3	100-160	0.75	212	58.1	10.58	0.734774	0.0016	
	ms4	100-160	0.6	227	48.5	13.56	0.738625	0.0020	
	bt			105	8.80	34.94	0.756920	0.0014	76.2 ± 1.2 Ma (+wr)
	plag			2.60	23.9	0.312	0.719029	0.0012	
	(ap)*			2.86	388	0.214	0.717169	0.0018	
	wr			96.9	166	1.689	0.720941	0.0020	

***Tab. 8.2**: Rb-Sr data of migmatites and mylonites of the Liquiñe migmatite dome. M = paramagnetic fraction (A as indicated, 13°), wr = whole rock, plag = plagioclase, ms = muscovite, bt = biotite, ap = apatite. (…)*: excluded from age calculation. See text for further details.*

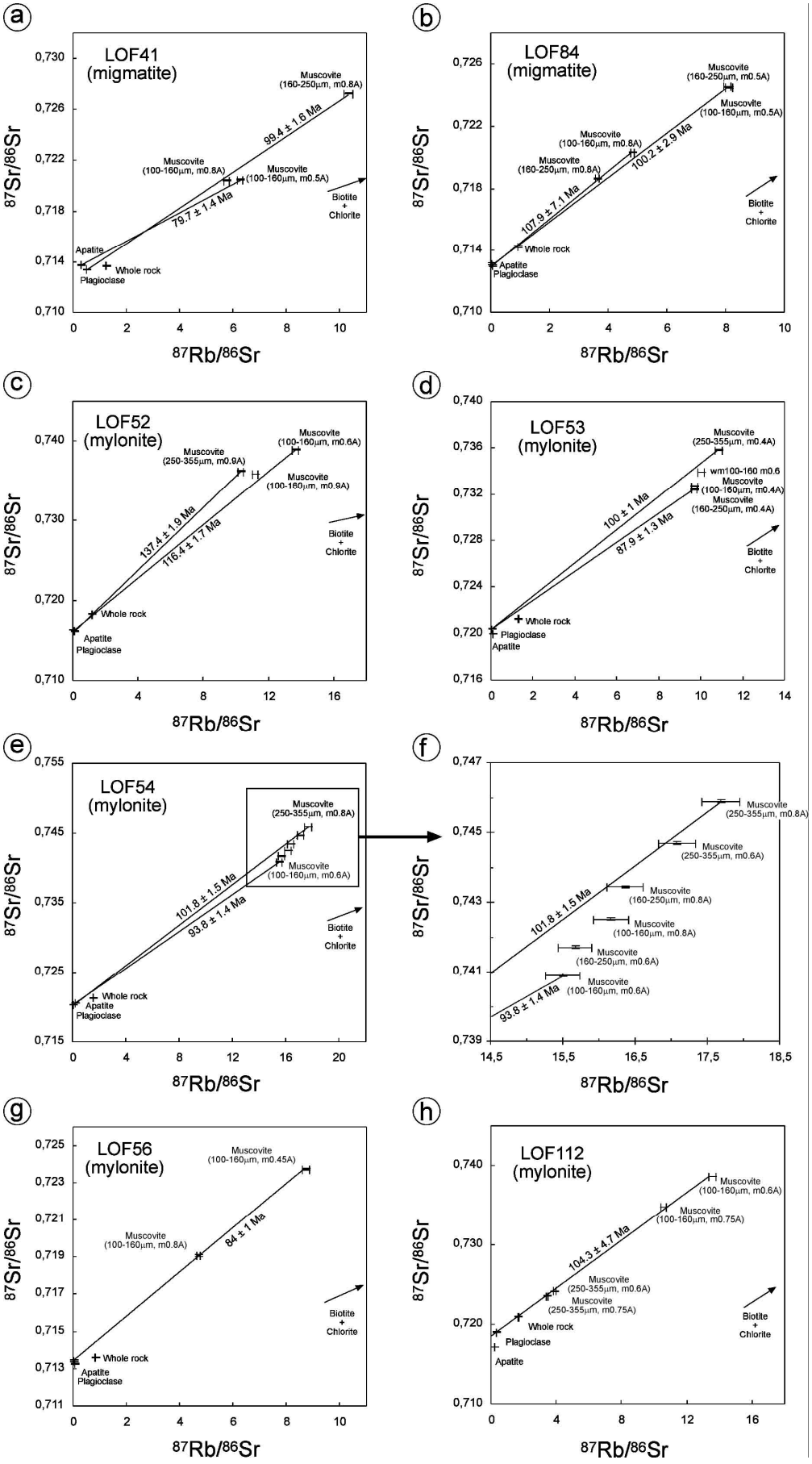

***Fig. 8.3**: Rb-Sr isotope systematics for samples of the Liquiñe migmatite dome.*

8.2.6 Discussion

Cooling ages versus deformation ages

The here presented isotopic data may be interpreted in two ways: either as cooling ages or as crystallization ages. The interpretation as cooling ages relies on the closure temperature concept formulated by Dodson (1973) and explains the obtained ages as the time at which the sample cooled through a specific temperature below which diffusion controlled loss of daughter nuclides from a specific phase is inhibited. For Sr-diffusion in muscovite, this closure temperature is ca. 550 ± 50°C (e.g. Cliff, 1985). However, more recent studies (e.g. Freeman et al., 1997, 1998, George and Bartlett, 1996, Hetzel and Glodny, 2002) showed that ductile deformation including dynamic recrystallization, nucleation of new grains, and grain boundary migration is an efficient mechanism to equilibrate the isotopic systems of all reorganized grains of a given rock volume. If such deformation takes place below the closure temperature, the isotopic clock will be reset to the time of deformation. Depending on the intensity of mylonitization, which is largely controlled by the strain rate and synkinematic temperature, the reset will be either partial if recrystallization is incomplete or total if all minerals are dynamically (re-)crystallized. Hetzel and Glodny (2002) reported data for both of these cases. They showed that amphibolite to greenschist facies ductile deformation even at relatively low strain rates can yield a perfect synkinematic Sr-isotopic reequilibration between muscovite, plagioclase, apatite, and whole rock when microtextural equilibrium is apparent in thin section. In this case, the isotopic data of a specific sample define an internal Rb/Sr mineral isochron which dates the cessation of ductile deformation. The interpretation of isotopic data is far less straight forward if textural disequilibria indicated by the existence of relic grains is apparent, because textural equilibrium is a prerequisite for isotopic equilibrium. In such a disequilibria case, mineral isotopic data are not expected to be consistent with a single isochron but should show a grain size dependence of apparent ages suggesting that deformation induced grain size reduction leaves “big” grains in which deformation induced isotopic resetting is less complete and/or ceases earlier than in smaller ones (Hetzel and Glodny, 2002, Freeman et al., 1997).

Migmatite samples

Samples LOF41 and LOF84 are from migmatites and show only minor indications of crystal plastic behaviour suggesting that they largely escaped post-migmatitic ductile deformation. However, both samples show isotope systematics inconsistent with a simple model of cooling from a high-grade metamorphic stage. Muscovites from sample LOF41 display a grainsize dependence of apparent ages with larger grains

recording older ages than smaller ones. The apatite, plagioclase and whole rock data suggest that isotopic homogenization may have been incomplete during the high-T event which led to the migmatization of the metasedimentary protolith. The apparent age of 99.4 ± 1.6 Ma derived by the combination of plagioclase with large muscovites may be interpreted as a minimal approximation of the time of migmatization if plagioclase grains are viewed as a reliable proxy for the synmigmatitic Sr composition. A higher amount of radiogenic Sr in apatite suggests a post-migmatitic partial reequilibration of this mineral eventually due to minor ductile deformation. If this interpretation is right, the apparent age of 79.7 ± 1.4 Ma obtained by the combination of apatite with small (100 – 160 μm) muscovites gives a maximal age of ductile deformation.

Isotopic data from sample LOF84 show a correlation between mica composition (paramagnetic fraction) and apparent age: Two grain size fractions of high paramagnetic muscovites define a regression line together with apatite, plagioclase, and whole rock data consistent with an age of 107.9 ± 8.1 Ma whereas two grain size fractions of low paramagnetic muscovites yield an isochron age of 100.2 ± 2.9 Ma if combined with apatite, plagioclase, and whole rock data. Since they are similar in age within the errors, both may approximate the time of cooling below 550 ± 50°C between 100 and 110 Ma.

Mylonite samples

Mylonite samples can be divided into low strain and high strain samples based on a subjective differentiation on microscale (relative grain size, existence of relic grains, intensity of penetrative foliation). Low strain mylonites (LOF52, LOF53, LOF54) display isotopic disequilibria which is consistent with the observation of textural disequilibria in thin sections. In these samples, plagioclase occurs dominantly as brittle clasts whereas muscovites show a bimodal grain size distribution with large grains interpreted as relicts of the migmatitic stage and fine grains crystallized during late stages of deformation. Consistently, muscovites show a correlation between grain size fraction and apparent age with larger grains showing older ages than younger ones indicating that grain size reduction due to mylonitization occurred. Hence, all obtained ages are mixed ages representing a prolonged mylonitization process after cooling of the protolith through 550 ± 50°C. In the samples LOF52 and LOF54, apatite Sr is more radiogenic than plagioclase Sr suggesting that apatite has been isotopically reequilibrated during deformation whereas plagioclase retained the pre-deformational isotopic signature. In sample LOF53, plagioclase shows more radiogenic Sr than apatite suggesting that the apatite Sr composition has been affected by sub-greenschistfacies alteration. In the low strain mylonite samples, apparent ages obtained by the

combination of (relic) plagioclase with large muscovites constrain the time of migmatization at the respective locations to be before or at 138.4 ± 1.9 Ma (LOF52), 100 ± 1 Ma (LOF53), and 101.8 ± 1.5 Ma (LOF54). The cessation of ductile deformation is constrained to be at or after 116.4 ± 1.7 Ma (LOF52), 87.9 ± 1.3 Ma (LOF53), and 93.8 ± 1.4 Ma (LOF54) considering small grain size fractions of muscovite and paragenetic apatite (in samples LOF52 and LOF54) and plagioclase (in sample LOF53).

High strain mylonites (LOF56 and LOF 112) yield mineral isochrones defined by 3 or more mineral fractions consistent with the minor occurrence of relic plagioclase and large mica grains. Sample LOF56 records syndeformational isotopic equilibrium between two paramagnetic muscovite fractions and apatite indicating cessation of ductile deformation at 84 ± 1 Ma at this location. Sample LOF112 records near syndeformational isotopic equilibration between muscovite, plagioclase, and whole rock, which define a regression line consistent with cessation of ductile deformation at 104.3 ± 4.7 Ma.

Sub-greenschist facies alteration

Apatite data

In the here presented data set, apatite has generally higher amounts of radiogenic Sr than plagioclase for a given sample most likely as a result of post-migmatitic greenschistfacies deformation which led to the recrystallization of apatite and reequilibration of its isotopic composition whereas plagioclase did not completely recrystallize synkinematically and retained its pre-deformational Sr isotopic signature. In two of seven samples (LOF53 and LOF112) however, apatite is poorer in radiogenic Sr with respect to the plagioclase. This exceptional behavior may be due to secondary epithermal processes which led to either recrystallization or neo-crystallization of hydrothermal apatite in equilibrium with a fluid which had a lower Sr initial isotopic composition than the pre-deformational mineral assemblage. Since the Sr initial isotopic signature of the protolith indicate a crustal source of Paleozoic age ($(^{87}Sr/^{86}Sr)_i$ = 0.713 – 0.720), any mantle derived fluid will have a significantly lower Sr isotopic signature ($(^{87}Sr/^{86}Sr)_i$ ~ 0.704, MORB). Dominantly mantle derived fluids are likely to be present in the magmatic arc setting due to continuous mafic underplating and minor crustal contamination.

Biotite/chlorite data

For a given sample, biotite/chlorite-whole rock pairs yield an age which is invariably younger than those determined for muscovite. Ages range between 41.1 and 82.2 Ma

with a large time gap between biotite and muscovite age in the same sample of ca. 15-50 Ma. These considerably younger ages are most likely related to a alteration effects.

Almost all samples show indications of a slight diaphtoritic overprint as evident from sericitization of feldspar and chloritization of biotite. This generally leads to an exchange of Sr between the mineral and the surrounding fluids, a process which produces rejuvenated apparent ages without a geologic significance.

Tectonic implications

The Sr isotopic data presented here suggest that ductile deformation in the Liquiñe area is largely coeval to migmatization and pluton emplacement and thus probably genetically linked. The following scenario for the formation of the Liquiñe migmatite dome is proposed: Migmatization of Paleozoic metapelitic country rocks took place during emplacement of parts of the North Patagonian Batholith between 100 and 140 Ma. The majority of samples (five of six) constrain migmatization to have occurred in the 100 – 105 Ma time interval. One sample (LOF52) represents a pre- to early migmatitic event at 135 – 140 Ma. Ductile deformation in the country rock induced by the granitoid emplacement is late- to postmigmatitic (ca. 105 – 80 Ma) and outlasted migmatization locally for ca. 20 Ma. The geologically active setting (magmatic arc) caused post-deformational fluid percolation which affected and obliterated the isotope systematics of biotite and, occasionally, of apatite.

8.3 Dating magmatism and metamorphism in the back-arc

In order to constrain the magmatic, metamorphic, and exhumation history of rocks of the Southern Andean back-arc and their relation with the Paleozoic basement of the fore-arc, two samples representative for the magmatic and of the metasedimentary back-arc basement have been dated using the Rb-Sr isotope method. The two samples were found close to the Chilean-Argentine border at 39°45’S. They originate from localities east of the active volcanic arc within the Neltume block (Ch. 4.4.4): 1. a feldspar-rich biotite-diorite (LOF19) which could be related either to mostly Devonian granitoids of the North Patagonian Massif (Argentina) or to the Permocarbonifereous magmatic belt paralleling the Gondwana margin in Chile; 2. a lower greenschist facies schist (LOF76) which could be related either to Permocarbonifereous rocks of the Eastern Series or to the metamorphic Rocks of North Patagonian Massif where peak metamorphism occurred during the Devonian.

8.3.1 Petrography

Magmatites

Sample LOF19 (UTM 283590E/5587924N) is a medium to coarse grained biotite-diorite from the shore of Lago Epulafquen in Argentina. At macroscale, the rock is isotropic, at microscale, however, a weak foliation defined by biotite can be recognized. Magmatically zoned plagioclase and biotite are the main mineral phases, quartz, apatite, titanite, opaques, and zircon are accessory phases. This magmatic mineral assemblage shows a gabbro-dioritic whole rock chemical composition (Tab. A5 in Appendix VI) with high contents of elements which are favorably incorporated in plagioclase and biotite (high-Ca, Na, K, Al, Ba, Sr). A very weak solid state deformation is indicated by undulose extinction of plagioclase and quartz, plagioclase shows magmatic zonation and occasionally kinked twins. An incipient diaphtoritic overprint is evidenced by slight chloritization of biotite and sericitization of plagioclase.

Metasediments

Sample LOF76 (UTM 269223E/5569426N) is a fine grained pelitic muscovite schist (phyllite) from east of Lago Pirihueico in Chile. The phyllite shows a very well developed crenulation cleavage and an associated lineation (Fig. 4.12). At microscale, quartz occurs as small grains elongated parallel to the cleavage, and shows minor indications for crystal plasticity like undulose extinction, deformation bands, and grain boundary migration. Remnants of plagioclase clasts are almost completely replaced by sericite, muscovite, chlorite, and quartz. Opaques are abundant, apatite is an accessory phase.

8.3.2 Analytical technique and results

For a detailed description of analytical techniques, see chapter 8.2.4 of this work. From sample LOF19, whole rock and mineral separates of plagioclase, apatite, and two grain size fractions of biotite were analyzed. From sample LOF76, six grain size and magnetically defined fractions of muscovite, three grain size fractions of chlorite-muscovite intergrowths, and whole rock were analyzed. The analytical results are summarized in Table 8.3 and visualized in Fig. 8.4.

Sample LOF19 yields an (imperfect) isochron age of 343.5 ± 8.4 Ma (2σ, MSWD = 199, $(^{87}Sr/^{86}Sr)_i = 0.70497$), defined by two sieve fractions of biotite (160-250 and 250-355 µm), plagioclase, apatite, and whole rock (Fig. 8.4a). Fine grained biotite (100-160

μm) plots slightly below the isochron and has not been included in the regression analysis.

Sample LOF76 gives an isochron age of 270 ± 22 Ma (2σ, MSWD = 0.61, $(^{87}Sr/^{86}Sr)_i$ = 0.7196) based on six sieve and paramagnetic fractions of muscovite (Fig. 8.4b). The whole rock data plot perfectly on the same isochron reflecting that the Rb-Sr budget of the rock is dominated by muscovite and that isotopic equilibrium was attained at handspecimen scale. If a regression is calculated considering the six muscovite fractions together with the whole rock data, the resulting isochron (270 ± 22 Ma (2σ), MSWD = 0.49, $(^{87}Sr/^{86}Sr)_i$ = 0.7196) is identical to the muscovite-only isochron. Three sieve fractions of chlorite (100-160, 160-250, and 250-355 μm) separated from this sample plot slightly below this isochron. A regression line calculated from these data is subparallel to the muscovite-based isochron and has a slope that corresponds to an age of 274 ± 38 Ma (2σ, MSWD = 0.49).

	Size (μm)	M (A)	Rb (ppm)	Sr (ppm)	$^{87}Rb/^{86}Sr$	$^{87}Sr/^{86}Sr$	$^{87}Sr/^{86}Sr$ $2\sigma_m$ (%)
LOF19	**(343.5 ± 8.4 Ma, $(^{87}Sr/^{86}Sr)_i$ = 0.70497)**						
bt1	250-355		274	55.8	14.30	0.775145	0.0058
bt2	160-250		214	70.3	8.853	0.747979	0.0014
(bt3)*	100-160		176	55.6	9.188	0.747608	0.0016
plag			54.3	939	0.167	0.705845	0.0014
ap			0.90	486	0.005	0.704643	0.0012
wr			121	931	0.376	0.707180	0.0024
LOF74	**(270 ± 22 Ma, $(^{87}Sr/^{86}Sr)_i$ = 0.7196)**						
ms1	250-355	1.3	286	95.8	8.659	0.753011	0.0016
ms2	250-355	0.8	324	102	9.279	0.755306	0.0016
ms3	160-250	1.3	311	115	7.895	0.749723	0.0016
ms4	160-250	0.8	325	119	7.952	0.750042	0.0016
ms5	100-160	1.3	295	116	7.390	0.748187	0.0016
ms6	100-160	0.8	325	123	7.674	0.749199	0.0012
(chl1)*	250-355		12.5	4.98	7.275	0.745474	0.0018
(chl2)*	160-250		11.6	4.01	8.380	0.749656	0.0016
(chl3)*	100-160		21.7	7.75	8.1310	0.748996	0.0028
(wr)*			176	61.9	8.263	0.751339	0.0018

Tab. 8.3*: Rb-Sr data of back-arc basement. Abbreviations: M = paramagnetic fraction (A as indicated, 13°), wr = whole rock, plag = plagioclase, ms = muscovite, chl = chlorite, bt = biotite, ap = apatite. (…)*: excluded from age calculation. See text for further details.*

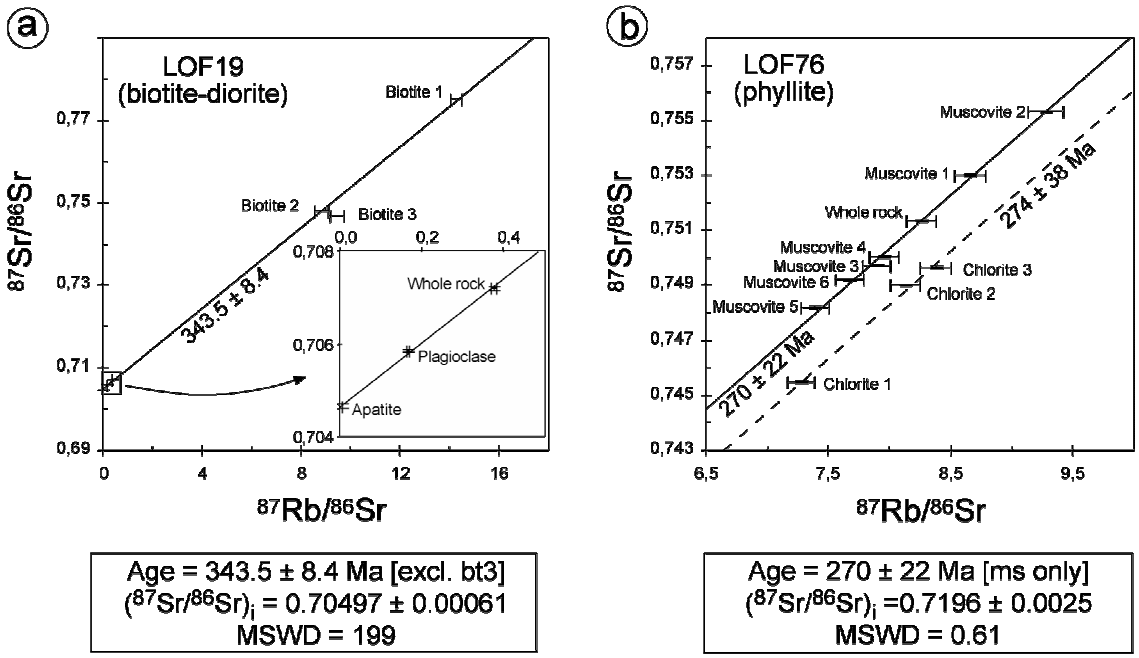

***Fig. 8.4**: Rb-Sr isochron plots for back-arc basement samples.*

8.3.3 Discussion

Magmatites

The Sr isotopic data of the biotite-diorite (LOF19) indicate a close approximation to chemical and isotopic equilibrium between apatite, plagioclase, biotite, and whole rock at ca. 344 ± 8 Ma. In the absence of significant ductile deformation, this age most likely reflects the time of crystallization of the biotite-diorite. The deviation of fine-grained biotite (< 160 µm) towards a lower apparent age may be due to minor alteration and/or later ductile deformation. The relatively low initial Sr isotopic composition ($^{87}Sr/^{86}Sr)_i$ = 0.70497) suggests that the melt most likely was dominated by a Neoproterozoic or Paleozoic mantle-derived addition to the crust. Regionally, metamorphic basement in this area is related to the North Patagonian Massif and of high-T, low-P type, characterized by the widespread occurrence of granitoids and migmatites (Ostera et al., 2001, Lucassen et al., subm., and references therein). Peak metamorphism occurred during the Devonian (370 - 380 Ma, Lucassen et al., subm.. Ostera et al., 2001). Crustal derived granitoids from the same area have Devonian (370 Ma, Linares et al., 1988) and Late Carboniferous to Permian ages (300 and 280 Ma, Lucassen et al. subm., Linares et al., 1988). The latter magmatic phase is generally related to a magmatic belt that developed at the southwestern margin of Gondwana outcropping dominantly in the Chilean fore-arc region (Rapela and Kay, 1988, Hervé et al., 1988, Cingolani et al., 1991, Lucassen et al., 1999). The here obtained Early Carboniferous crystallization age

thus closes the gap between Devonian and Permocarboniferous magmatism and related high-T, low-P metamorphism in the Southern Andean back-arc. This suggests that crustal growth by magmatic addition was a long-term process active between Devonian and Permian times for nearly 100 Ma.

Metasediments

Isotopic data of the phyllite sample (LOF76) indicate internal isotopic equilibrium within the rock at 270 ± 22 Ma. The chlorite data are interpreted as reflecting post-equilibrium open system behaviour of this phase. Metasedimentary rocks with Permocarboniferous ages of metamorphism are well known from the fore-arc Coastal Cordillera north of 38°S (Hervé, 1977, Hervé et al., 1988, Glodny et al., 2002) and from the western foothills of the Main Cordillera (Martin et al., 1999). These metasedimentary rocks are described as the Eastern Series (Hervé, 1977) and represent continent (Gondwana)-derived detritus deposited in an marginal marine environment (Martin et al., 1999), intruded by granitoids of the Permocarboniferous magmatic arc, the ages of which cluster around 300 Ma (Lucassen et al., subm., and references therein). Lucassen et al. (subm.) reported a Late Carboniferous and a Permian age (298 and 264 Ma) for low-grade shales from the Eastern Series in the Coastal Cordillera near 36.5°S (Sierra Nahuelbuta) and interpreted these ages as reflecting, respectively, the thermal overprint of late Paleozoic magmatism and a late stage tectonic overprint. The here obtained Permian age expands the dataset of Lucassen et al. (subm.) and suggests that also metasedimentary rocks of the Southern Andean back-arc share are common PT evolution with low-grade rocks of the Eastern Series of the fore-arc with respect to their Permocarboniferous metamorphic history. Paleozoic rocks of the Coastal Cordillera and of the western foothills of the Main Cordillera are unconformably overlain by Middle Triassic sediments (Ferraris, 1981, Martin et al., 1999) indicating that the fore-arc has been exhumed during the Early Triassic. Since this exhumation occurred regionally along the Gondwana margin (Martin et al., 1999) it is plausible that the back-arc basement was also exhumed by Early Triassic times.

Tectonic implication

The Sr isotopic data presented here suggest that pre-Andean back-arc basement has a similar magmatic, metamorphic, and exhumation history like Paleozoic basement rocks of the fore-arc region. If so, the Southern Andean back-arc, like the fore-arc, did not experience significant regional exhumation after the Triassic and remains in a tectonically stable position since.